

Inducing Oxygen Vacancies to Modulate Ignition Threshold of Nanothermites

Feiyu Xu, Prithwish Biswas, Pankaj Ghildiyal, and Michael R. Zachariah*

Cite This: *Energy Fuels* 2022, 36, 5878–5884

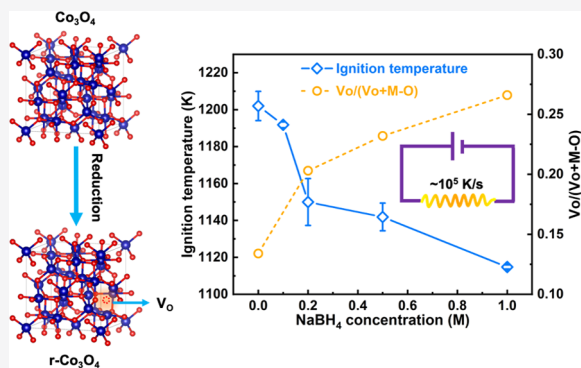
Read Online

ACCESS |

Metrics & More

Article Recommendations

ABSTRACT: Many characteristics of metal oxides are governed by defect chemistry. As a result, defect engineering has become an effective strategy to modulate the electrical, optical, and mechanical properties of metal oxides. As the most commonly used oxidizers in nanothermite systems, metal oxides offer an opportunity to manipulate nanothermite reactions from a fundamental, atomic-scale, defect structure aspect. However, the challenge lies in the complexity of nanothermite reactions that requires shifting defect equilibria without introducing other variations. In this work, we choose a model oxidizer Co_3O_4 for aluminum-based nanothermite systems due to its easily tunable oxygen nonstoichiometry. Utilizing a soft chemistry reduction process, oxygen vacancies are created in Co_3O_4 with minimal structural disturbance. Ignition threshold is used as a metric to probe the effect of oxygen defects. The results show an inverse correlation between the ignition temperature of $\text{Al}/\text{Co}_3\text{O}_4$ nanothermites and oxygen vacancy content in Co_3O_4 . The evolved species analyzed by temperature-jump time-of-flight mass spectrometry (T -jump TOFMS) indicates that the ignition is likely limited by the availability of sufficient gas-phase oxygen species, the production of which can be facilitated by oxygen vacancies.



1. INTRODUCTION

Nanothermites are nanostructured fuel and oxidizer composites that store a large amount of chemical energy and release it vigorously upon ignition, typically in the form of heat.^{1–4} It has become an emerging class of energetic materials that offer both high energy density and fast energy release.^{5–8} Aluminum is a benchmark fuel used in nanothermites, while a variety of oxidizers offer tunability and multifunctionality to nanothermite systems. Metal oxides are frequently adopted as oxidizers (i.e., oxygen donors) in nanothermite systems, and their electrical, optical, and mechanical properties are strongly governed by defects. One of the most important point defects in metal oxides is oxygen vacancy, which has been demonstrated to play an important role in photocatalysis,^{9,10} oxygen evolution reaction (OER)/oxygen reduction reaction (ORR),^{11,12} and gas sensing applications of metal oxides.¹³

Nanothermite reactions are complex as many factors including the intrinsic properties of fuel and oxidizer, surface area, and porosity have a cooperative impact on reaction characteristics. Thus, to investigate the impact of defects on nanothermite reactions, other variables of the system must remain unchanged. For reducible metal oxides such as Co_3O_4 , Fe_2O_3 , MnO_2 , etc., due to multiple available valence states of metal ions, the generation of oxygen vacancies can be accommodated, to some extent, by a deviation from stoichiometry. Typical methods to create oxygen vacancies

include annealing in reducing atmosphere,¹⁴ argon plasma etching,¹⁵ and chemical reduction,^{16,17} most of which are under aggressive conditions that are detrimental to nanostructures. For example, elevated temperature tends to cause particle sintering, leading to loss of surface area, and eventually results in inferior performance of nanothermites.¹⁸ Reaction with Ar plasma also changes the morphology and surface area of nanoparticles.¹⁵ On the other hand, NaBH_4 reduction is a solution-based room-temperature process that can provide access to metastable phases while preserving the pristine structure of nanoparticles.^{19,20}

The attempt to investigate the relationship between oxygen vacancies in metal oxides and ignition of nanothermites has previously been made via aliovalent cation substitution in fluorites and perovskites.^{21,22} The results show systematic trends in how the atomic properties of metal oxides can regulate the ignition threshold via oxygen transport in the condensed phase.^{23,24} However, doping often causes multiple

Received: February 21, 2022

Revised: April 25, 2022

Published: May 13, 2022



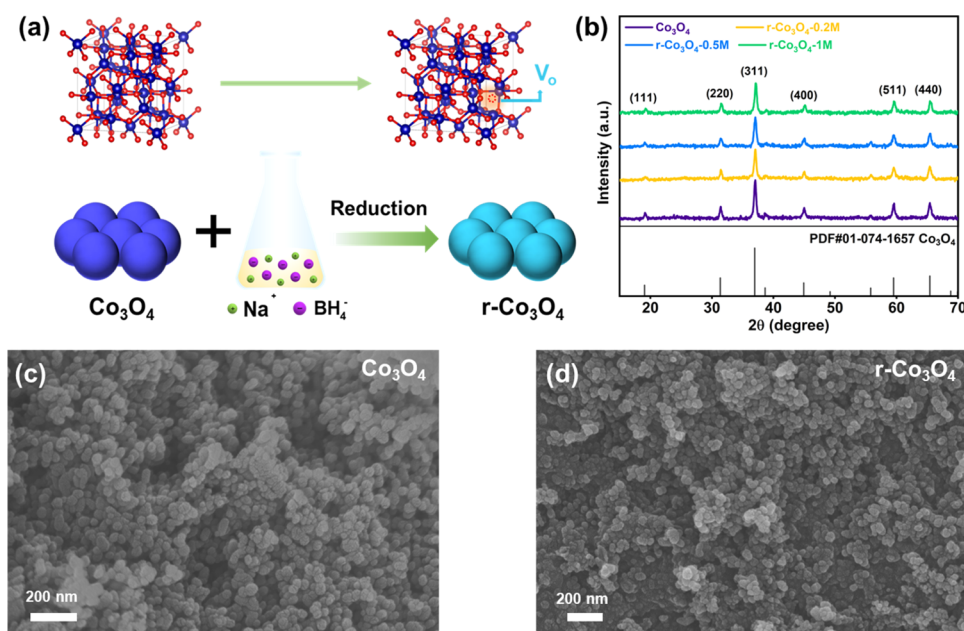


Figure 1. (a) Schematic illustration of the room-temperature solution-based NaBH_4 reduction of Co_3O_4 , which generates oxygen vacancies and results in oxygen-deficient $\text{r-Co}_3\text{O}_4$. (b) Powder X-ray diffraction pattern of the standard cubic spinel Co_3O_4 , pristine Co_3O_4 , and $\text{r-Co}_3\text{O}_4$. (c) Scanning electron microscopic (SEM) image of Co_3O_4 and (d) $\text{r-Co}_3\text{O}_4$ nanoparticles.

structural changes that are coupled with each other, making it challenging to isolate the effect of individual factors. Further, the behavior of metal oxides in nanothermite reactions is diverse and not fully represented by prior studies. For example, previous works are based on the condensed-phase transport of oxygen, but oxygen can be transferred to fuel via gas phase as well.²⁵ It is also of practical significance to explore more commonly used simple metal oxides.

In this work, Co_3O_4 is selected as a model oxidizer due to its tunable oxygen nonstoichiometry,^{15,20} with the provision to connect oxygen defects in metal oxides with the ignition threshold of nanothermites. We utilize a low-temperature NaBH_4 reduction procedure to create oxygen-deficient Co_3O_4 , without causing structural rearrangement of the crystal. Quantitative analysis of X-ray photoelectron spectroscopy (XPS) results indicates that the amount of oxygen vacancies is related to reductant concentration. Further, temperature-jump (T -jump) ignition measurements show an inverse correlation between the ignition temperature of $\text{Al/Co}_3\text{O}_4$ nanothermite and oxygen vacancy content in Co_3O_4 . Probing of reaction intermediates by time-resolved mass spectrometry suggests a gaseous oxygen-initiated ignition, and oxygen vacancies seem to facilitate the release of molecular oxygen from Co_3O_4 .

2. EXPERIMENTAL SECTION

2.1. Materials. Aluminum nanopowders (80 nm, 66.7 wt % active content) were purchased from Novacentrix. Co_3O_4 nanoparticles (<50 nm) and NaBH_4 were purchased from Sigma-Aldrich. CoO nanoparticles (<50 nm) were purchased from U.S. Research Nanomaterials Inc.

2.2. Synthesis of Oxygen-Deficient Co_3O_4 . To prepare oxygen-deficient $\text{r-Co}_3\text{O}_4$ NPs, NaBH_4 was used to partially reduce pristine Co_3O_4 NPs and introduce oxygen vacancies into the lattice structure,¹⁹ as illustrated in Figure 1a. The overall reaction is shown in eq 1



First, NaBH_4 was dissolved in deionized (DI) water at concentrations varying from 0.1 to 1 M. Fifty milligrams of as-received Co_3O_4 nanoparticles were then immersed in 10 mL of as-prepared NaBH_4 solution for 1 h. The resultant dispersion was centrifuged at 10 000 rpm for 10 min, followed by washing with DI water 3 times and ethanol 2 times to remove residual ions and separate the particles. Finally, the collected powders were dried in a vacuum oven for 12 h. A series of experiments were carried out by varying the concentration of NaBH_4 aqueous solution at room temperature to tune the extent of reduction and thus the oxygen nonstoichiometry in $\text{r-Co}_3\text{O}_4$. The resultant samples are denoted by $\text{r-Co}_3\text{O}_{4-c}$, where c is the concentration of the NaBH_4 solution used to prepare the sample.

2.3. Characterizations. Powder X-ray diffraction (PANalytical EMPYREAN, $\text{Cu K}\alpha$ source ($\lambda = 1.543 \text{ \AA}$)) was performed to characterize the crystal structure of metal oxide nanoparticles. The morphology of metal oxide nanoparticles was characterized by SEM (Nova NanoSEM 450) and transmission electron microscopy (TEM) (Thermo Scientific Talos L120C, accelerating voltage 120 kV). The size distribution was obtained using a Nano Measurer 1.2 from an ensemble of 200 particles. A Kratos AXIS ULTRA^{DL}D XPS system equipped with an $\text{Al K}\alpha$ X-ray source and a 165 mm mean radius electron energy hemispherical analyzer were employed to examine the surface species of metal oxide nanoparticles.

2.4. Temperature-Jump (T -Jump) Fast Heating Experiments. Temperature-jump (T -jump) fast heating experiments including ignition temperature measurement and time-of-flight mass spectrometry (TOFMS) were used to investigate $\text{Al/Co}_3\text{O}_4$ reactions.^{26,27} For a typical measurement, the sample powder was dispersed in hexane via sonication and coated on an $\sim 1 \text{ cm}$ platinum wire ($d = 76 \text{ }\mu\text{m}$) with a micropipette. During the measurement, the Pt wire was resistively heated to $\sim 1400 \text{ K}$ by a 3 ms pulse to ignite the sample. The temperature of the wire can be determined by the Callendar–Van Dusen equation from the I – V curve of the wire recorded by an oscilloscope. For ignition measurements, the sample holder was placed in a pressurizable chamber that was kept in vacuum. The ignition event was captured by a Vision Research Phantom v12.0 digital camera (frame rate = 67 000 fps) from the observation window to determine the onset of ignition. The sample holder was inserted into a time-of-flight mass spectrometer for evolved species analysis, and time-resolved mass spectra were collected at an interval of 100 μs .

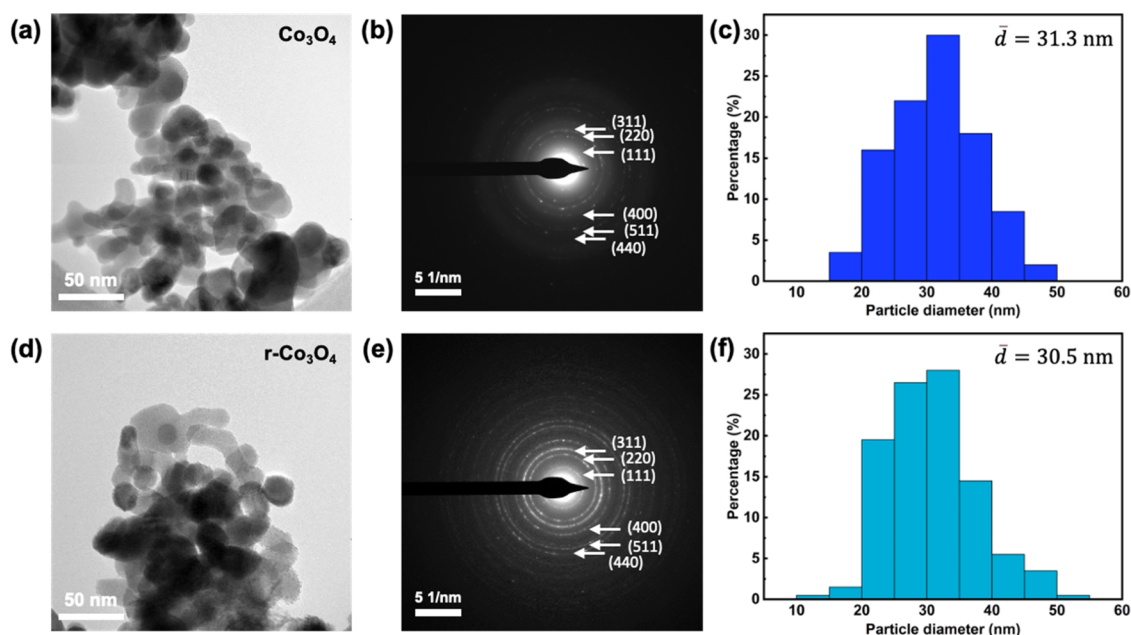


Figure 2. TEM images of (a) Co_3O_4 and (d) $\text{r-Co}_3\text{O}_4$ show similar particle morphology. SAED patterns of (b) Co_3O_4 and (e) $\text{r-Co}_3\text{O}_4$ match the XRD results and indicate that they have the same crystal structure. Size distributions of (c) Co_3O_4 and (f) $\text{r-Co}_3\text{O}_4$ particles show mean diameters of 31.3 and 30.5 nm, respectively.

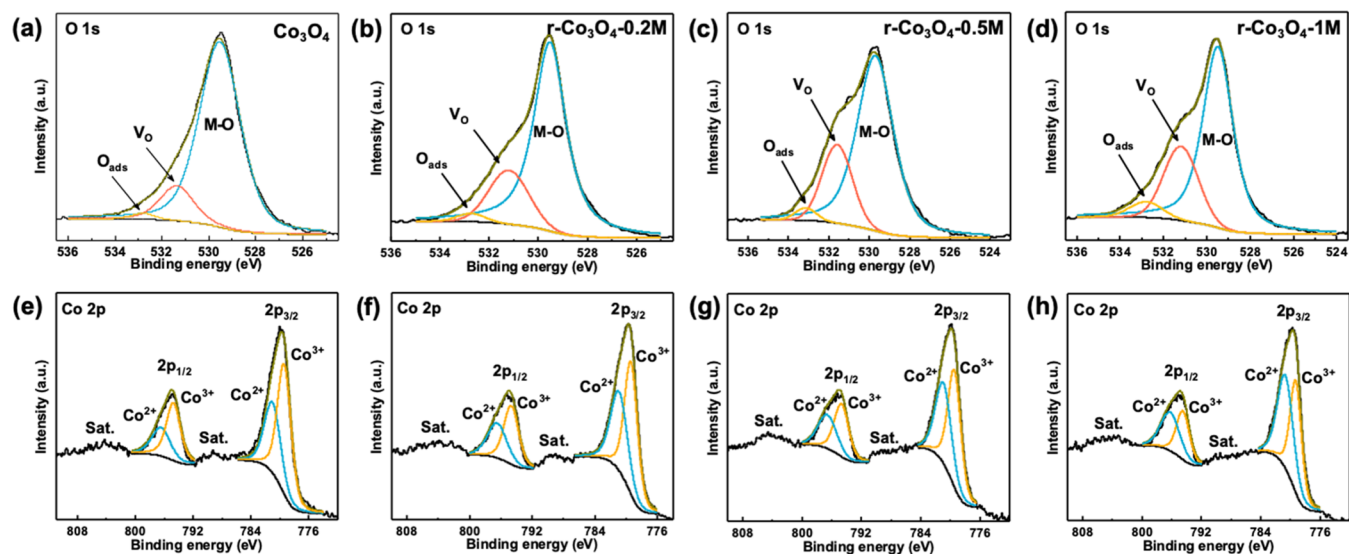


Figure 3. High-resolution O 1s (top) and the corresponding Co 2p (bottom) spectra of Co_3O_4 and $\text{r-Co}_3\text{O}_4$ samples. The spectra are deconvoluted using Voigt line shapes. A shoulder peak emerges after NaBH_4 reduction in O 1s spectra as a result of the increased intensity of the component peak indicative of oxygen defects.

3. RESULTS AND DISCUSSION

X-ray diffraction (XRD) patterns (Figure 1b) of the pristine and as-prepared samples can be indexed to spinel Co_3O_4 . The results indicate that after NaBH_4 treatment, there is no observable structural rearrangement in $\text{r-Co}_3\text{O}_4$ crystals. The removal of oxygen has minimal effect on XRD results because the scattering of incident X-ray mainly depends on electron density; thus, the contribution from oxygen ions is relatively small. Scanning electron microscopy (SEM) and transmission electron microscopy (TEM) were used to characterize the morphology and size distributions of Co_3O_4 NPs before and after reduction.

Micrographs of Co_3O_4 and $\text{r-Co}_3\text{O}_4$ -1M NPs (Figures 1c,d and 2a,d) show similar spherical morphology, with an average particle size of 31.3 and 30.5 nm (Figure 2c,f), respectively, indicating negligible size difference before and after reduction. Select area electron diffraction (SAED) patterns (Figure 2b,e) match the XRD results and confirm that the mild reduction process does not induce any changes in the crystal structure.

Since the reduction process will change the oxidation state of cations and lead to the formation of anion vacancies, surface compositions of Co_3O_4 and $\text{r-Co}_3\text{O}_4$ NPs were analyzed by X-ray photoelectron spectroscopy (XPS). High-resolution O 1s and Co 2p spectra of Co_3O_4 and $\text{r-Co}_3\text{O}_4$ samples are shown in Figure 3. O 1s spectrum of pristine Co_3O_4 has a single peak. An additional shoulder peak appears in O 1s spectra of $\text{r-Co}_3\text{O}_4$

Co_3O_4 after NaBH_4 reduction. Doublet peaks due to spin-orbit splitting and shake-up satellite structures are observed for Co 2p spectra.²⁸ To identify the surface species, Shirley background was applied, and the spectra were deconvoluted using Voigt line shapes.²⁹ The O 1s spectra were fit into three component peaks at 529.5, 531, and 533.2 eV. The most prominent peak at 529.5 eV corresponds to stoichiometric oxygen (M–O). The peak at a slightly higher binding energy indicates nonstoichiometric oxygen, which are associated with the presence of oxygen vacancies (V_{O}). The third peak is due to adsorbed oxygen species (O_{ads}). The interpretation of the O 1s spectra of Co_3O_4 is consistent with previously reported results.^{28,30} According to the deconvolution results, the newly emerged shoulder peak arises from the increase in the V_{O} constituent of the spectra. To compare the extent of reduction by different concentrations of NaBH_4 , quantitative analysis was performed for both O 1s and Co 2p spectra. Areas under individual characteristic peaks were used to represent the relative content of that species. The ratios of $V_{\text{O}}/(V_{\text{O}} + \text{M–O})$ and $\text{Co}^{2+}/\text{Co}^{3+}$ were calculated and are tabulated in Table 1.

Table 1. Co_3O_4 XPS Results: Relative Ratio of Surface Species

sample	$V_{\text{O}}/(V_{\text{O}} + \text{M–O})$ (%)	$\text{Co}^{2+}/\text{Co}^{3+}$
Co_3O_4	13.4	0.64
r- Co_3O_4 -0.2M	20.3	0.77
r- Co_3O_4 -0.5M	23.2	0.83
r- Co_3O_4 -1M	26.6	1.14

As shown in the table, the relative amount of V_{O} increases with the NaBH_4 concentration, accompanied by an increasing $\text{Co}^{2+}/\text{Co}^{3+}$ ratio as a result of maintaining charge neutrality.

It should be noted that although XPS is typically considered as a surface characterization technique, in this case, since the particles are nanosized and have a considerable surface-to-volume ratio, the source of the signal could be ambiguous. The sampling depth of XPS is typically considered $3\lambda_i$, where λ_i is the inelastic mean free path (IMFP) of an electron in a solid. For Co_3O_4 and Al $K\alpha$ sources, λ_i of electrons emitted from O 1s orbitals (B.E. ≈ 530 eV) was calculated to be ~ 1.8 nm using NIST Electron Inelastic-Mean-Free-Path Database: version 1.2. Thus, the XPS sampling depth for Co_3O_4 should be around 5.4 nm. If we assume a particle size of 30 nm, the sampling volume would be $\sim 74\%$ of the particle. This suggests that the discussion of oxygen vacancies should not only be limited to the surface but also be limited to the subsurface (bulk) region.

Heating rate has a strong effect on the onset temperature of thermally activated reactions. Considering the high exothermicity and rapidity of nanothermite reactions, a temperature-jump (T -jump) setup was used to measure ignition temperature at a comparably high heating rate of $\sim 3 \times 10^5$ K/s.^{26,31} A representative temperature vs time profile in T -jump experiments is shown in Figure 4a. The ignition time was visually determined from high-speed imaging. To investigate the effect of oxygen vacancies on ignition, the ignition temperature (T_{ign}) and estimated V_{O} percentage ($V_{\text{O}}\%$) were plotted together for different NaBH_4 concentrations. As shown in Figure 4b, there is a clear inverse correlation between T_{ign} and $V_{\text{O}}\%$. Snapshots

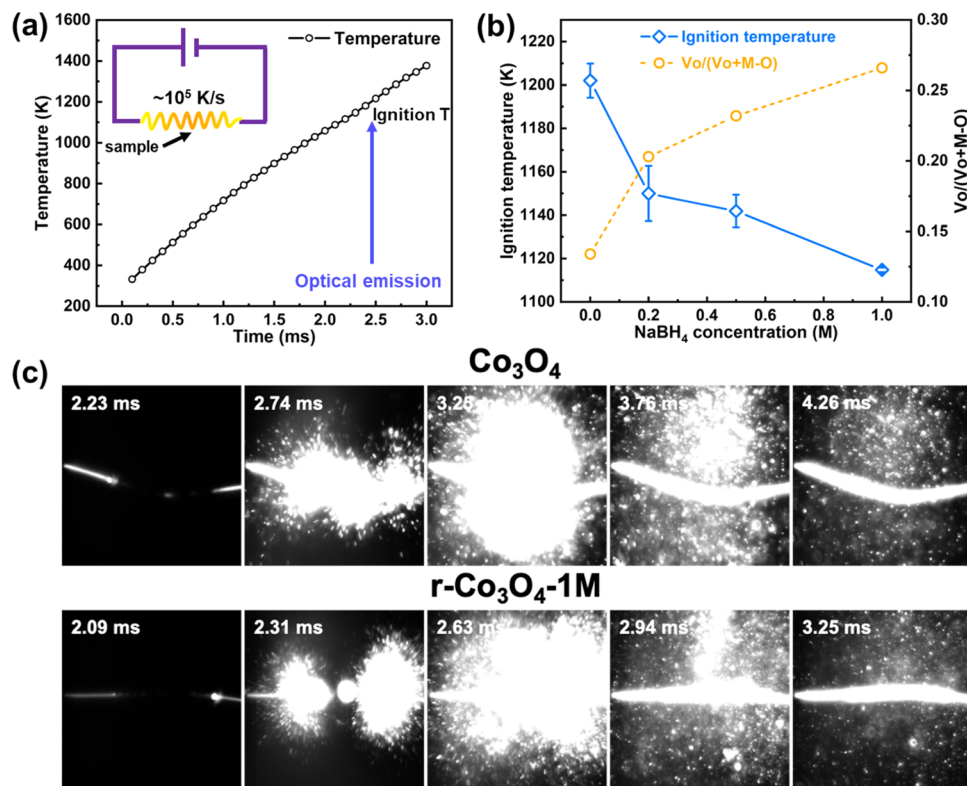


Figure 4. (a) Temporal temperature profile of Al/ Co_3O_4 in T -jump ignition measurements. The ignition temperature was determined by optical emission to be 1200 K. The rest of the T -jump measurements are conducted at a similar heating rate on the order of 10^5 K/s. (b) Ignition temperature of Al/ Co_3O_4 nanothermites and relative content of oxygen vacancies in Co_3O_4 show an inverse correlation. (c) Snapshots from high-speed imaging of Al/ Co_3O_4 and Al/r- Co_3O_4 -1M ignitions. The nanothermite reaction seems equally violent after NaBH_4 reduction.

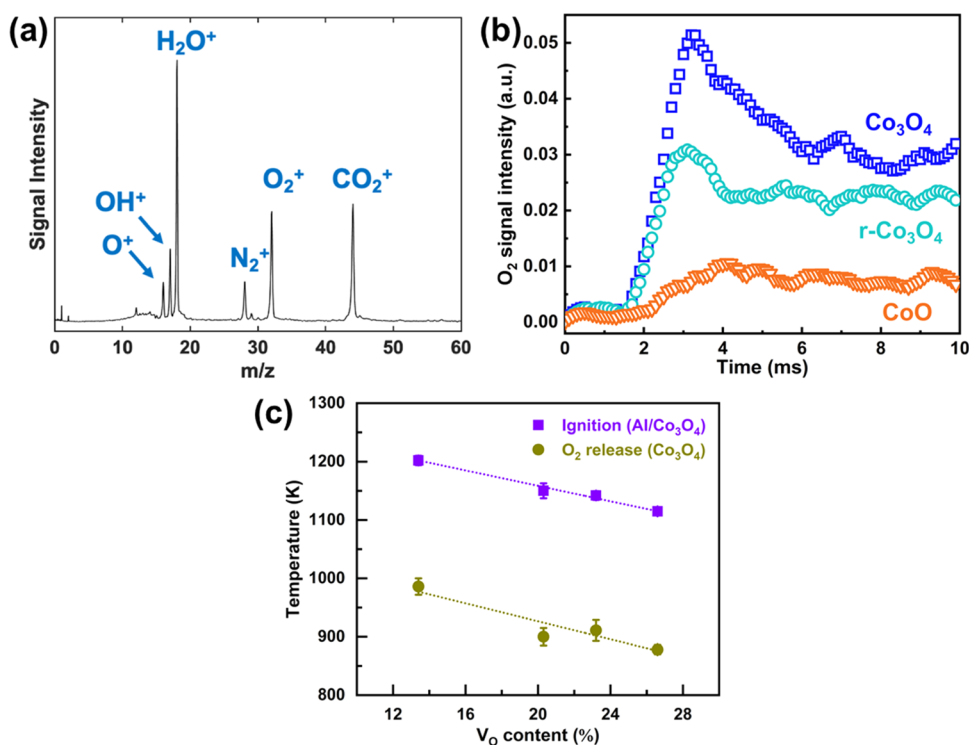


Figure 5. (a) Summary plot of time-resolved mass spectra of r-Co₃O₄-1M obtained under fast heating (integrated over 10 ms). (b) O₂⁺ ($m/z = 32$) signals from Co₃O₄, r-Co₃O₄-1M, and CoO, the relative intensity of which confirms oxygen deficiency in r-Co₃O₄. (c) Correlation of the ignition temperature of Al/Co₃O₄ and Al/r-Co₃O₄ samples and onset temperature of O₂ release from Co₃O₄ and r-Co₃O₄ samples with oxygen vacancy content.

from the high-speed videos (Figure 4c) of Al/Co₃O₄ and Al/r-Co₃O₄ ignitions show that, at least visually, the NaBH₄ reduction process does not have any substantial impact on reactivity. This is expected as only a relatively small number of oxygen ions were removed under mild conditions, leaving the rest of the oxide structure undisturbed.

The initiation of nanothermite reactions can be categorized into two groups based on how oxygen is transferred to the fuel: condensed-phase-dominated and gas-phase-dominated. To determine which type of reaction leads to the ignition of Al/Co₃O₄, we couple the temperature-jump (T -jump) fast heating technique with time-resolved time-of-flight mass spectrometry (TOFMS) to analyze the evolved reaction intermediate and product species.^{26,27} Figure 5a shows a typical mass spectrum of r-Co₃O₄-1M under fast heating. Background species such as H₂O⁺ ($m/z = 18$), OH⁺ ($m/z = 17$), N₂⁺ ($m/z = 28$), and CO₂⁺ ($m/z = 44$) can be observed, consistent with previous results.³¹ A weak C₂H₅⁺ ($m/z = 29$) signal most likely comes from physisorbed ethanol. The oxidation of carbonaceous impurities will also contribute to CO₂⁺ and H₂O⁺ signals. As mentioned above, O₂⁺ ($m/z = 32$) species is critical in determining the ignition mechanism. In this reaction, O₂ is released as Co₃O₄ decomposes and forms CoO. The release profiles of O₂ from Co₃O₄, r-Co₃O₄-1M, and CoO are plotted in Figure 5b. The relative intensity of their signals shows that the amount of oxygen generated from Co₃O₄ > r-Co₃O₄-1M > CoO, which confirms the oxygen deficiency in r-Co₃O₄.

The ignition temperature of Al/Co₃O₄ and Al/r-Co₃O₄ samples, as well as the onset temperature of O₂ release from Co₃O₄ and r-Co₃O₄, is shown in Figure 5c. Overall, the oxygen release temperature is about 200–250 K lower than the ignition temperature of the corresponding nanothermite,

which suggests that the ignition occurred with the presence of gaseous O₂. The lag between oxygen release from the oxidizer and ignition of nanothermite is somewhat unusual. However, since the initial step of Co₃O₄ decomposition to CoO only liberates ~25% of the oxygen at maximum, the lag might be due to low oxygen availability at the early stage of decomposition. As shown in Figure 5c, r-Co₃O₄ samples have lower oxygen release temperature compared with pristine Co₃O₄, which is likely the reason for the decreased ignition temperature of Al/r-Co₃O₄ nanothermites. It is worth noting, though, that if the extent of reduction is too high and phase transformation to lower valence state oxide occurs, it will negate the lowering effect of oxygen vacancies on ignition temperature. In fact, the ignition temperature of Al/CoO is 1223 K, which is slightly higher than that of Al/Co₃O₄ (1202 K). This indicates that the transformation of Co³⁺ to Co²⁺ is not responsible for the reduced ignition temperature. Instead, it is the induced oxygen vacancies that result in the lowered ignition temperature.

The thermolysis of metal oxides typically involves the diffusion of lattice oxygen to surface, where electrons are transferred, leading to cation reduction, and oxygen is released in its molecular form (some studies also indicate the generation of atomic oxygen, which may later combine and form molecular oxygen).^{32,33} The above process is illustrated in Figure 6. The overall kinetics of these complex processes may be controlled by oxygen vacancy-mediated diffusion steps or by desorption of surface oxygen. Previous work reported that the effective activation energy for oxygen release from metal oxide NPs at a high heating rate is much lower than that at a low heating rate.³⁴ For example, the activation energy for O₂ release from Co₃O₄ at a high heating rate ($\sim 10^5$ K/s) is 77

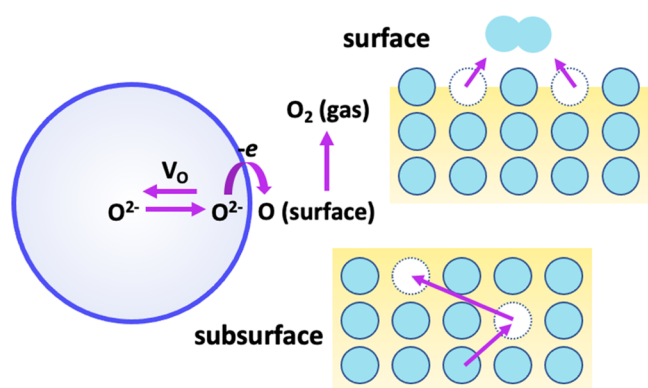


Figure 6. Schematic illustration of the oxygen release pathway from Co_3O_4 . Typically, subsurface (bulk) oxygen ions diffuse to the surface via a vacancy hopping mechanism. Then, oxygen ions lose electrons and desorb as atomic or molecular oxygen at the surface.

versus 269 kJ/mol at a low heating rate (10 K/min).³⁴ It was postulated that at a high heating rate the oxygen release is limited by the intraparticle diffusion of oxygen. In this study, ignition and oxygen release were also measured at a high heating rate and an increased oxygen vacancy density can facilitate the transport of subsurface oxygen ions, which is typically represented by oxygen ion conductivity (σ)²³

$$\sigma = Z_q[V_{\text{O}}^{\bullet\bullet}]\mu \quad (2)$$

Z_q is the effective charge of oxygen ion, $[V_{\text{O}}^{\bullet\bullet}]$ is the oxygen vacancy concentration, and μ is the oxygen ion mobility. Besides, as oxygen ions diffuse toward the surface, oxygen vacancies will diffuse inward and promote oxygen ion transport in regions where V_{O} concentration is initially low. Further, as most surface chemistry occurs at defect sites, the desorption of oxygen molecules may also benefit from more surface oxygen vacancies.

4. CONCLUSIONS

The effect of oxygen vacancies on the ignition threshold of nanothermites was investigated using a model oxide Co_3O_4 , with which tunable oxygen vacancy generation can be achieved via a room-temperature NaBH_4 reduction procedure, without altering the morphology or crystal structure of Co_3O_4 . T -Jump ignition measurements show an inverse correlation between ignition temperature and oxygen vacancy concentration. Further analysis of reaction intermediates indicates a gas-phase-dominated initiation, and lower O_2 release onset temperature is responsible for decreased ignition temperature. The promoted O_2 release is attributed to oxygen vacancies facilitating the vacancy-mediated transport of oxygen ions in Co_3O_4 . The results demonstrate that defect engineering could be a promising strategy for modulating the performance of nanothermites.

AUTHOR INFORMATION

Corresponding Author

Michael R. Zachariah – University of California, Riverside, California 92551, United States; orcid.org/0000-0002-4115-3324; Email: mrz@engr.ucr.edu

Authors

Feiyu Xu – University of California, Riverside, California 92551, United States; University of Maryland, College Park, Maryland 20742, United States

Prithwish Biswas – University of California, Riverside, California 92551, United States; orcid.org/0000-0002-9921-2905

Pankaj Ghildiyal – University of California, Riverside, California 92551, United States; University of Maryland, College Park, Maryland 20742, United States; orcid.org/0000-0002-4422-3068

Complete contact information is available at:

<https://pubs.acs.org/10.1021/acs.energyfuels.2c00502>

Notes

The authors declare no competing financial interest.

ACKNOWLEDGMENTS

The authors acknowledge support from the ONR and DTRA-MSEE URA.

REFERENCES

- Yetter, R. A. Progress towards Nanoengineered Energetic Materials. *Proc. Combust. Inst.* **2021**, *38*, 57–81.
- Ma, X.; Li, Y.; Hussain, I.; Shen, R.; Yang, G.; Zhang, K. Core–Shell Structured Nanoenergetic Materials: Preparation and Fundamental Properties. *Adv. Mater.* **2020**, *32*, No. 2001291.
- Comet, M.; Martin, C.; Schnell, F.; Spitzer, D. Nanothermites: A Short Review. Factsheet for Experimenters, Present and Future Challenges. *Propellants, Explos., Pyrotech.* **2019**, *44*, 18–36.
- He, W.; Liu, P.-J.; He, G.-Q.; Gozin, M.; Yan, Q.-L. Highly Reactive Metastable Intermixed Composites (MICs): Preparation and Characterization. *Adv. Mater.* **2018**, *30*, No. 1706293.
- Dreizin, E. L. Metal-Based Reactive Nanomaterials. *Prog. Energy Combust. Sci.* **2009**, *35*, 141–167.
- Khasainov, B.; Comet, M.; Veysiere, B.; Spitzer, D. Comparison of Performance of Fast-Reacting Nanothermites and Primary Explosives. *Propellants, Explos., Pyrotech.* **2017**, *42*, 754–772.
- Ghildiyal, P.; Ke, X.; Biswas, P.; Nava, G.; Schwan, J.; Xu, F.; Kline, D. J.; Wang, H.; Mangolini, L.; Zachariah, M. R. Silicon Nanoparticles for the Reactivity and Energetic Density Enhancement of Energetic-Biocidal Mesoparticle Composites. *ACS Appl. Mater. Interfaces* **2021**, *13*, 458–467.
- Biswas, P.; Ghildiyal, P.; Kwon, H.; Wang, H.; Alibay, Z.; Xu, F.; Wang, Y.; Wong, B. M.; Zachariah, M. R. Rerouting Pathways of Solid-State Ammonia Borane Energy Release. *J. Phys. Chem. C* **2022**, *126*, 48–57.
- Huang, Y.; Yu, Y.; Yu, Y.; Zhang, B. Oxygen Vacancy Engineering in Photocatalysis. *Sol. RRL* **2020**, *4*, No. 2000037.
- Jia, J.; Qian, C.; Dong, Y.; Feng, L.; Wang, H.; Ghossoub, M.; T. Butler, K.; Walsh, A.; A. Ozin, G. Heterogeneous Catalytic Hydrogenation of CO₂ by Metal Oxides: Defect Engineering – Perfecting Imperfection. *Chem. Soc. Rev.* **2017**, *46*, 4631–4644.
- Ji, Q.; Bi, L.; Zhang, J.; Cao, H.; S. Zhao, X. The Role of Oxygen Vacancies of ABO₃ Perovskite Oxides in the Oxygen Reduction Reaction. *Energy Environ. Sci.* **2020**, *13*, 1408–1428.
- Xu, W.; Lyu, F.; Bai, Y.; Gao, A.; Feng, J.; Cai, Z.; Yin, Y. Porous Cobalt Oxide Nanoplates Enriched with Oxygen Vacancies for Oxygen Evolution Reaction. *Nano Energy* **2018**, *43*, 110–116.
- Dey, A. Semiconductor Metal Oxide Gas Sensors: A Review. *Mater. Sci. Eng. B* **2018**, *229*, 206–217.
- Chen, X.; Liu, L.; Yu, P. Y.; Mao, S. S. Increasing Solar Absorption for Photocatalysis with Black Hydrogenated Titanium Dioxide Nanocrystals. *Science* **2011**, *331*, 746–750.
- Xu, L.; Jiang, Q.; Xiao, Z.; Li, X.; Huo, J.; Wang, S.; Dai, L. Plasma-Engraved Co₃O₄ Nanosheets with Oxygen Vacancies and

High Surface Area for the Oxygen Evolution Reaction. *Angew. Chem.* **2016**, *128*, 5363–5367.

(16) Ou, G.; Xu, Y.; Wen, B.; Lin, R.; Ge, B.; Tang, Y.; Liang, Y.; Yang, C.; Huang, K.; Zu, D.; Yu, R.; Chen, W.; Li, J.; Wu, H.; Liu, L.-M.; Li, Y. Tuning Defects in Oxides at Room Temperature by Lithium Reduction. *Nat. Commun.* **2018**, *9*, No. 1302.

(17) Bao, J.; Zhang, X.; Fan, B.; Zhang, J.; Zhou, M.; Yang, W.; Hu, X.; Wang, H.; Pan, B.; Xie, Y. Ultrathin Spinel-Structured Nanosheets Rich in Oxygen Deficiencies for Enhanced Electrocatalytic Water Oxidation. *Angew. Chem.* **2015**, *127*, 7507–7512.

(18) Sullivan, K. T.; Piekiet, N. W.; Wu, C.; Chowdhury, S.; Kelly, S. T.; Hufnagel, T. C.; Fezzaa, K.; Zachariah, M. R. Reactive Sintering: An Important Component in the Combustion of Nanocomposite Thermites. *Combust. Flame* **2012**, *159*, 2–15.

(19) Zhuang, L.; Ge, L.; Yang, Y.; Li, M.; Jia, Y.; Yao, X.; Zhu, Z. Ultrathin Iron-Cobalt Oxide Nanosheets with Abundant Oxygen Vacancies for the Oxygen Evolution Reaction. *Adv. Mater.* **2017**, *29*, No. 1606793.

(20) Wang, Y.; Zhou, T.; Jiang, K.; Da, P.; Peng, Z.; Tang, J.; Kong, B.; Cai, W.-B.; Yang, Z.; Zheng, G. Reduced Mesoporous Co₃O₄ Nanowires as Efficient Water Oxidation Electrocatalysts and Supercapacitor Electrodes. *Adv. Energy Mater.* **2014**, *4*, No. 1400696.

(21) Luo, G.; Wang, X.; Zachariah, M. R.; Mishra, R. Ignition Threshold of Perovskite-Based Oxides for Solid Fuel Oxidation from First-Principles Calculations. *J. Phys. Chem. C* **2019**, *123*, 17644–17649.

(22) Wang, X.; Zachariah, M. R. What Atomic Properties of Metal Oxide Control the Reaction Threshold of Solid Elemental Fuels? *Phys. Chem. Chem. Phys.* **2018**, *20*, 26885–26891.

(23) Wang, X.; Wu, T.; Zachariah, M. R. Doped Perovskites To Evaluate the Relationship between Fuel–Oxidizer Thermite Ignition and Bond Energy, Electronegativity, and Oxygen Vacancy. *J. Phys. Chem. C* **2017**, *121*, 147–152.

(24) Wang, X.; Zhou, W.; DeLisio, J. B.; Egan, G. C.; Zachariah, M. R. Doped δ -Bismuth Oxides to Investigate Oxygen Ion Transport as a Metric for Condensed Phase Thermite Ignition. *Phys. Chem. Chem. Phys.* **2017**, *19*, 12749–12758.

(25) Jian, G.; Chowdhury, S.; Sullivan, K.; Zachariah, M. R. Nanothermite Reactions: Is Gas Phase Oxygen Generation from the Oxygen Carrier an Essential Prerequisite to Ignition? *Combust. Flame* **2013**, *160*, 432–437.

(26) Zhou, L.; Piekiet, N.; Chowdhury, S.; Zachariah, M. R. Time-Resolved Mass Spectrometry of the Exothermic Reaction between Nanoaluminum and Metal Oxides: The Role of Oxygen Release. *J. Phys. Chem. C* **2010**, *114*, 14269–14275.

(27) Jian, G.; Piekiet, N. W.; Zachariah, M. R. Time-Resolved Mass Spectrometry of Nano-Al and Nano-Al/CuO Thermite under Rapid Heating: A Mechanistic Study. *J. Phys. Chem. C* **2012**, *116*, 26881–26887.

(28) Chuang, T. J.; Brundle, C. R.; Rice, D. W. Interpretation of the X-Ray Photoemission Spectra of Cobalt Oxides and Cobalt Oxide Surfaces. *Surf. Sci.* **1976**, *59*, 413–429.

(29) Major, G. H.; Fairley, N.; Sherwood, P. M. A.; Linford, M. R.; Terry, J.; Fernandez, V.; Artyushkova, K. Practical Guide for Curve Fitting in X-Ray Photoelectron Spectroscopy. *J. Vac. Sci. Technol., A* **2020**, *38*, No. 061203.

(30) Oku, M.; Sato, Y. In-Situ X-Ray Photoelectron Spectroscopic Study of the Reversible Phase Transition between CoO and Co₃O₄ in Oxygen of 10–3 Pa. *Appl. Surf. Sci.* **1992**, *55*, 37–41.

(31) Zhou, L.; Piekiet, N.; Chowdhury, S.; Zachariah, M. R. T-Jump/Time-of-Flight Mass Spectrometry for Time-Resolved Analysis of Energetic Materials. *Rapid Commun. Mass Spectrom.* **2009**, *23*, 194–202.

(32) Malinin, G. V.; Tolmachev, Y. M. Thermal Decomposition of Solid Metal Oxides. *Russ. Chem. Rev.* **1975**, *44*, 392–397.

(33) Galwey, A. K.; Brown, M. E. *Thermal Decomposition of Ionic Solids: Chemical Properties and Reactivities of Ionic Crystalline Phases*; Elsevier, 1999.

(34) Jian, G.; Zhou, L.; Piekiet, N. W.; Zachariah, M. R. Low Effective Activation Energies for Oxygen Release from Metal Oxides: Evidence for Mass-Transfer Limits at High Heating Rates. *ChemPhysChem* **2014**, *15*, 1666–1672.

Recommended by ACS

Atomic Scale Characterization of Fluxional Cation Behavior on Nanoparticle Surfaces: Probing Oxygen Vacancy Creation/Annihilation at Surface Sites

Ethan L. Lawrence, Peter A. Crozier, *et al.*

JANUARY 28, 2021

ACS NANO

READ 

In Situ Observation of Nanoparticle Exsolution from Perovskite Oxides: From Atomic Scale Mechanistic Insight to Nanostructure Tailoring

Dragos Neagu, Mihalis N. Tsampas, *et al.*

OCTOBER 21, 2019

ACS NANO

READ 

Sintering Mechanism of Core@Shell Metal@Metal Oxide Nanoparticles

Namsoon Eom, Knut Deppert, *et al.*

JULY 14, 2021

THE JOURNAL OF PHYSICAL CHEMISTRY C

READ 

Nanoparticle Size Effects on Phase Stability for Molybdenum and Tungsten Carbides

Anukriti Shrestha, Christopher Paolucci, *et al.*

JUNE 09, 2021

CHEMISTRY OF MATERIALS

READ 

Get More Suggestions >